

PVLM: Parsing-Aware Vision Language Model with Dynamic Contrastive Learning for Zero-Shot Deepfake Attribution

Yaning Zhang , Jiahe Zhang, Chunjie Ma , Weili Guan , Member, IEEE, Tian Gan , Zan Gao , Senior Member, IEEE

Abstract—The challenge of tracing the source attribution of forged faces has gained significant attention due to the rapid advancement of generative models. However, existing deepfake attribution (DFA) works primarily focus on the interaction among various domains in vision modality, and other modalities such as texts and face parsing are not fully explored. Besides, they tend to fail to assess the generalization performance of deepfake attributors to unseen advanced generators like diffusion in a fine-grained manner. In this paper, we propose a novel parsing-aware vision language model with dynamic contrastive learning (PVLM) method for zero-shot deepfake attribution (ZS-DFA), which facilitates effective and fine-grained traceability to unseen advanced generators. Specifically, we conduct a novel and fine-grained ZS-DFA benchmark to evaluate the attribution performance of deepfake attributors to unseen advanced generators like diffusion. Besides, we propose an innovative parsing-guided vision language model with dynamic contrastive learning (PVLM) method to capture general and diverse attribution features. We are motivated by the observation that the preservation of source face attributes in facial images generated by GAN and diffusion models varies significantly. We employ the inherent face attributes preservation differences between GAN and diffusion face images to capture face parsing-aware forgery representations. Therefore, we devise a novel parsing encoder to focus on global face attribute embeddings, enabling parsing-guided DFA representation learning via dynamic vision-parsing matching. Additionally, we present a novel deepfake attribution contrastive center loss to pull relevant generators closer and push

This work was supported in part by the National Natural Science Foundation of China (No.62372325, No.62402255), Natural Science Foundation of Tianjin Municipality (No.23JCZDJC00280), Shandong Provincial Natural Science Foundation (No.ZR2024QF020), Shandong Province National Talents Supporting Program (No.2023GJLJRC-070), Shandong project towards the integration of education and industry (No.801822020100000024), Young Talent of Lifting engineering for Science and Technology in Shandong (No. SDAST2024QTB001), Shandong Project towards the Integration of Education and Industry (No.2024ZDZX11) (Corresponding author: Zan Gao)

Y. Zhang is with Faculty of Computer Science and Technology, Qilu University of Technology (Shandong Academy of Sciences), Jinan, 250014, China. E-mail: zhangyaning0321@163.com

J. Zhang is with Shandong University of Science and Technology, Jinan, 250031, China. E-mail: zhangjiahe00600@163.com.

C. Ma is with the Shandong Artificial Intelligence Institute, Qilu University of Technology (Shandong Academy of Sciences), Jinan, 250014, China. E-mail: mcj@machunjie.com

W. Guan is with the School of Electronics and Information Engineering, Harbin Institute of Technology, Shenzhen 150001, China. E-mail: guanweili@hit.edu.cn

T. Gan is with the School of Computer Science and Technology, Shandong University, Qingdao, 266237, China. E-mail: gantian@sdu.edu.cn

Z. Gao is with Shandong Artificial Intelligence Institute, Qilu University of Technology (Shandong Academy of Sciences), Jinan, 250014, China, and also with the Key Laboratory of Computer Vision and System, Ministry of Education, Tianjin University of Technology, Tianjin, 300384, China. E-mail: zangaonsh4522@gmail.com

irrelevant ones away, which can be introduced into DFA models to enhance traceability. Experimental results show that our model exceeds the state-of-the-art on the ZS-DFA benchmark via various protocol evaluations. Codes will be available at GitHub.

Index Terms—Deepfake attribution, zero-shot learning, vision language model, multi-perspective interaction, dynamic contrastive learning.

I. INTRODUCTION

With the proliferation of advanced generative frameworks, including generative adversarial networks (GANs) [1] and diffusion models [2], maliciously fabricated deepfake content on social platforms has raised significant concerns over facial integrity and personal privacy [3]. As a result, tracing the source of deepfakes has become a critical and urgent issue. Deepfake attribution (DFA) aims to identify and attribute forged faces using deep learning-based methods. Although current DFA techniques [4], [5] have made significant progress, they predominantly assume a closed-world setting where the training and testing sets share identical category distributions. This assumption limits their applicability in open-world scenarios, where novel forgery attacks continuously emerge. To overcome this problem, open-world deepfake attribution (OW-DFA) leverages unlabeled data in open-world contexts, to enhance attribution performance for forgery faces created by both seen and unseen generators. However, most DFA models [6], [7] focus solely on the interaction between image and frequency information within the visual modal, neglecting other modalities such as fine-grained text and face parsing, which may hinder generalization to unseen generators. For instance, DNA-Det [5] identifies globally consistent forgery features using the image modality for GAN architecture attribution. MPSL [7] further explores multi-scale image and frequency relationships among samples, enabling the attribution of both GAN and diffusion-generated face images [8]. However, they struggle to evaluate the generalization to unseen generators in a fine-grained manner.

To alleviate the limitations, we introduce a novel task, namely, zero-shot deepfake attribution (ZS-DFA). As Fig. 1 shows, unlike current deepfake attribution tasks (See Fig. 1 (a)) that conduct coarse-grained attribution performance evaluation on unseen GAN generators, our ZS-DFA task (See Fig. 1 (b)) aims to identify advanced unseen generators such as diffusion, fine-grainedly. Specifically, as shown in Fig. 2 (a), ZS-DFA encompasses about 20 advanced generators, categorized into

three manipulations such as entire face synthesis (EFS), face swap (FS), and attribute manipulation (AM). The challenge of ZS-DFA is how to design an attributor to mine general and discriminative forgery attribution traces synthesized by seen generators, to enhance the attribution performance for fake faces created by unseen advanced ones.

Inspired by the contrastive language-image pre-training (CLIP) model [9] which excels at zero-shot learning, we propose a parsing-aware vision language model with dynamic contrastive learning (PVLM) framework. Unlike CLIP which only focuses on image and text modals for zero-shot classification in general natural image scenarios, our PVLM model introduces fine-grained text and face parsing modalities, to enhance the learning of multiple-perspective (i.e., image, noise, and edge) visual features via cross-modality matching and dynamic cross-perspective alignment, to achieve fine-grained ZS-DFA. Specifically, our PVLM method differs from CLIP in the following points (See Fig. 2): First, since most face manipulations such as FS struggle to preserve facial attributes of the source image like eyebrows and eyes [3], as shown in Fig. 1, we employ a face parser [10] to generate parsing images to focus on different facial attribute regions. We observe that there are significant differences between pristine and forged face parsing images (See Fig. 1). Specifically, authentic face parsing images exhibit more precise attribute areas (e.g., eyes and eyebrows) than forged ones. Besides, parsing images derived from GAN-generated faces retain more accurate semantic attributes than those extracted from diffusion faces. Based on the observation, we propose a parsing encoder (PE) to capture global face parsing features, guiding our PVLM model to learn discriminative and general DFA embeddings. Second, we design a multi-perspective visual encoder (MPVE) to explore global and diverse multi-view (i.e., image, edge, and noise) forgery representations via the multi-head interaction module (MMI), as there are significant discrepancies between real and fake images in both edge and noise views [11], [12]. We present a novel dynamic cross-perspective contrastive loss to achieve dynamic vision-parsing matching. We also propose a language encoder to extract fine-grained language attribution embeddings for comprehensive vision-language matching. Finally, to enhance the ZS-DFA capability, we design a novel deepfake attribution contrastive center (DFACC) loss (See Fig. 2 (f)). Unlike the vanilla contrastive center loss [13] which enforces intra-generator compactness and inter-generator separability, our loss minimizes the distance between samples within the generator, while bringing related samples across generators closer and pushing unrelated ones farther apart. In summary, the contributions of our work are as follows:

- To the best of our knowledge, we conduct the first zero-shot fine-grained deepfake attribution benchmark, which contains novel and advanced generators like diffusion, to facilitate the ZS-DFA application in open-world scenarios where innovative face forgery generators emerge.

- We propose a novel parsing-aware vision language model with dynamic contrastive learning (PVLM) deepfake attributor, which introduces fine-grained text and face parsing modalities to enhance the learning of visual forgery features across image, noise, and edge views, thus mining both general and

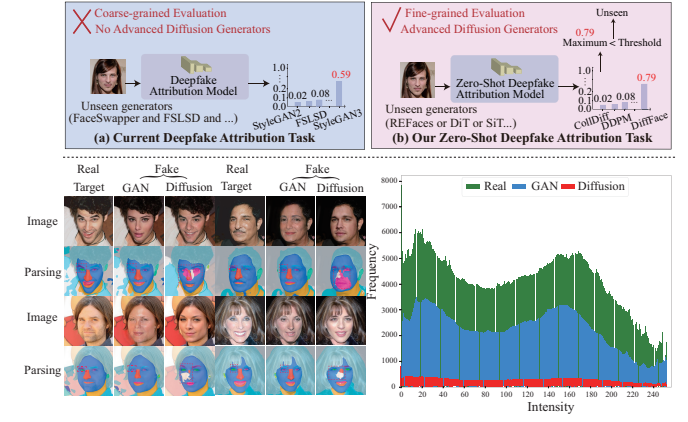


Fig. 1. Up: The overview of the deepfake attribution task. Down: Illustration of the face attribute-sensitive trait. Left: The visualization of real, GAN, and diffusion face parsing images. Right: The feature distribution histogram of real, GAN, and diffusion face parsing images.

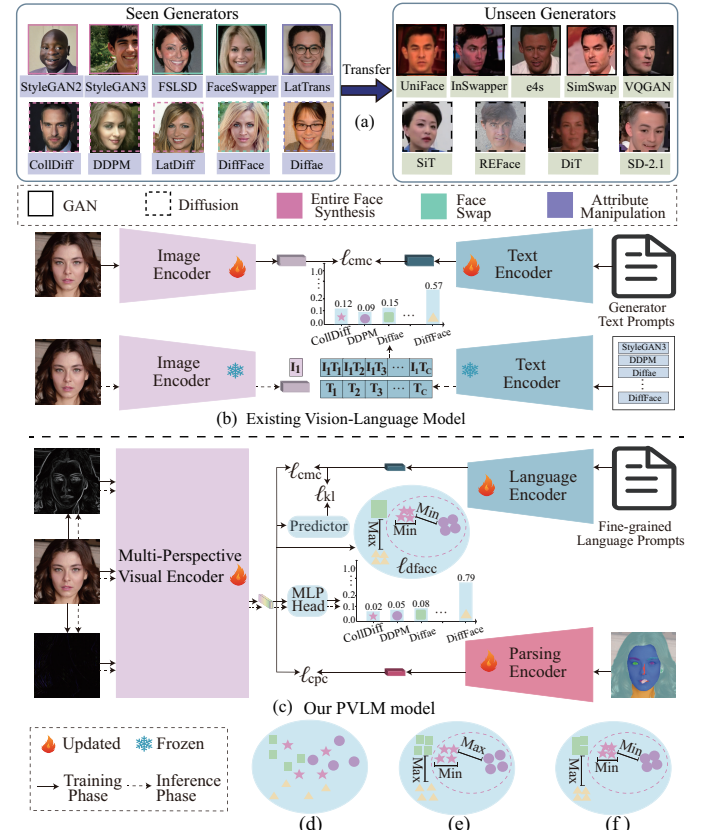


Fig. 2. (a) In ZS-DFA tasks, training and testing datasets are derived from distinct domains, with generators in the testing dataset being unseen during training. (b) Existing vision-language foundation model CLIP. (c) The proposed PVLM model. (d) Original DFA feature space. (e) DFA feature space supervised by vanilla contrastive center loss. (f) DFA feature space supervised by our DFACC loss.

discriminative attribution patterns.

- We propose a plug-and-play deepfake attribution contrastive center criterion to realize flexible intra-generator compactness and inter-generator separability, which could be integrated into any deepfake attributors to improve traceability.
- Experiments conducted on our benchmark demonstrate that our PVLM method surpasses the state of the art in zero-shot deepfake attribution scenarios.

II. RELATED WORK

Deepfake Attribution. DFA aims to identify the source of deepfake images through deep learning-based models, which is a challenging task due to the sophistication of deepfake technology. Most existing efforts [5], [4], [6], [14] focus on attributing GAN-generated content, with little attention given to more recent advanced generators like diffusion. DNA-Det [5] is designed to capture globally consistent architecture traces via pre-training on image transformation classification and patch-based contrastive learning. Sun et al. [6] propose a contrastive pseudo learning (CPL) network for OW-DFA tasks, which evaluates attribution performance against various GAN-generated face images. To address the limitation, MPSL [7] models global multi-scale image and frequency relations among samples, to attribute fake images generated by diffusion models. DE-FAKE [4] employs the CLIP model to attribute fake images created by diffusion text-to-image generation models. However, they struggle to fully explore fine-grained text and vision modalities, and assess the generalization performance of deepfake attributors to unseen generators in a fine-grained manner. By contrast, we conduct the bi-modal (i.e., parsing and text) guided multi-view (i.e., image, edge, and noise) visual forgery representation learning, to realize fine-grained ZS-DFA.

Zero-Shot Learning. Zero-Shot learning (ZSL) enables a model to recognize and classify instances from unseen classes during the training phase. Traditionally, ZSL [15], [16] for image classification relies on learning auxiliary attributes rather than predefined class labels. Predictions are made by evaluating the similarity between image and text embeddings, derived from encoding both images and textual class descriptions [17]. Existing approaches like CLIP [9] tend to train image and text encoders to learn joint representations. Recent works [18], [19] have focused on improving zero-shot classification performance of CLIP by enhancing textual descriptions. In this work, we are the first to attain excellent zero-shot performance for DFA. Unlike CLIP which focuses solely on image-text matching, our PVLM method captures diverse global visual forgery features across image, noise, and edge perspectives, performing both vision-parsing matching and vision-language alignment to explore comprehensive and model-agnostic forensic representations.

III. METHODOLOGY

A. Problem Definition

For ZS-DFA, given a seen domain (X_s, Y_s) and an unseen domain (X_u, Y_u) , the input distributions of the seen and unseen domains are distinct, and there is no intersection between their label spaces, i.e. $X_s \neq X_u$ and $Y_s \cap Y_u = \emptyset$, where X denotes the input distribution and Y represents the label space. ZS-DFA aims to learn a deepfake attributor, trained on the seen domain, to classify the distribution from the unseen domain. In our work, we employ the training set $(I_s, y_s) \in \mathcal{D}_{\text{tra}}$ from the seen domain to train our model, and test it using the testing set $(I_u, y_u) \in \mathcal{D}_{\text{tes}}$ from the unseen domain, where I denotes the input image, $y \in \{\mathbf{e}_i \mid \mathbf{e}_i = (0, 0, \dots, 1, \dots, 0), 1 \leq i \leq x\}$

denotes generator-specific one-hot labels, $\mathbf{e}_i \in \mathbb{R}^x$ represents the i -th one-hot label, and x is the number of generators.

B. Method Overview

Unlike prior methods [5], [9] that focus on integrations within vision or vision-language modalities for DFA, our PVLM model pioneers the joint interactions of vision, language, and face parsing modalities to realize ZS-DFA. As Fig. 3 shows, our method includes three modules: multi-perspective visual encoder (MPVE), parsing encoder (PE), and language encoder (LE).

During training, given an input facial appearance image I^a , we leverage the Sobel operator [20], SRM [21], face parser [10], and fine-grained text generator [12] to obtain the edge image I^e , noise image I^n , parsing image P , and fine-grained attribution prompts T , respectively. Subsequently, I^a , I^e , and I^n are fed into the MPVE to capture global visual attribution embeddings I_v across three views. Meanwhile, PVLM transmits P and T to PE and LE, to extract the diverse global parsing features P_g and language attribution ones T_l , accordingly. Thereafter, we conduct the language-guided and parsing-guided contrastive learning, and flexible metric learning, respectively. Meanwhile, PVLM sends I_v to the predictor and MLP, both consisting of fully connected layers, to yield the predicted language embeddings T_l^{pre} and deepfake attribution ones, separately. Finally, we leverage the softmax function to produce the prediction y_{pre} .

During inference, to prevent information leakage, PVLM merely uses MPVE to dig visual features across three views, which are then imparted to the MLP head and softmax function, to yield the prediction.

C. Multi-Perspective Visual Encoder

To capture comprehensive and general visual attribution embeddings, we propose the MPVE module, since global representations are helpful for DFA as proven by [5]. Unlike existing multi-domain DFA methods [7], [22] which tend to focus on the interaction between the local frequency and RGB information, our MPVE module can dig appearance global forgery traces, fine-grained noise global representations, and edge global features, and integrate them to explore diverse and common visual embeddings across three views. As shown in Fig. 3, MPVE mainly includes an appearance encoder (AE), an edge encoder (EE), a noise encoder (NE), and a multi-view multi-head interaction (MMI) module.

To extract global appearance forgery features, we design AE, which consists of a backbone with stacked convolutional layers followed by a transformer encoder (TE) with several transformer blocks, following [23]. Particularly, given an input face appearance image $I^a \in \mathbb{R}^{3 \times H \times W}$, AE derives the local feature map $I_{\text{loc}}^a \in \mathbb{R}^{c \times h \times w}$ via the backbone, where H and W denote the height and width of the image, and c, h, w are the channel, height, and width of the feature map, respectively. AE then sends it to the TE, to investigate global relationships among feature patches, to yield global appearance DFA embeddings $I_g^a \in \mathbb{R}^{2 \times d}$, where d denotes the dimension of the embeddings. AE obtains appearance class token $I_{\text{cls}}^a \in \mathbb{R}^{1 \times d}$

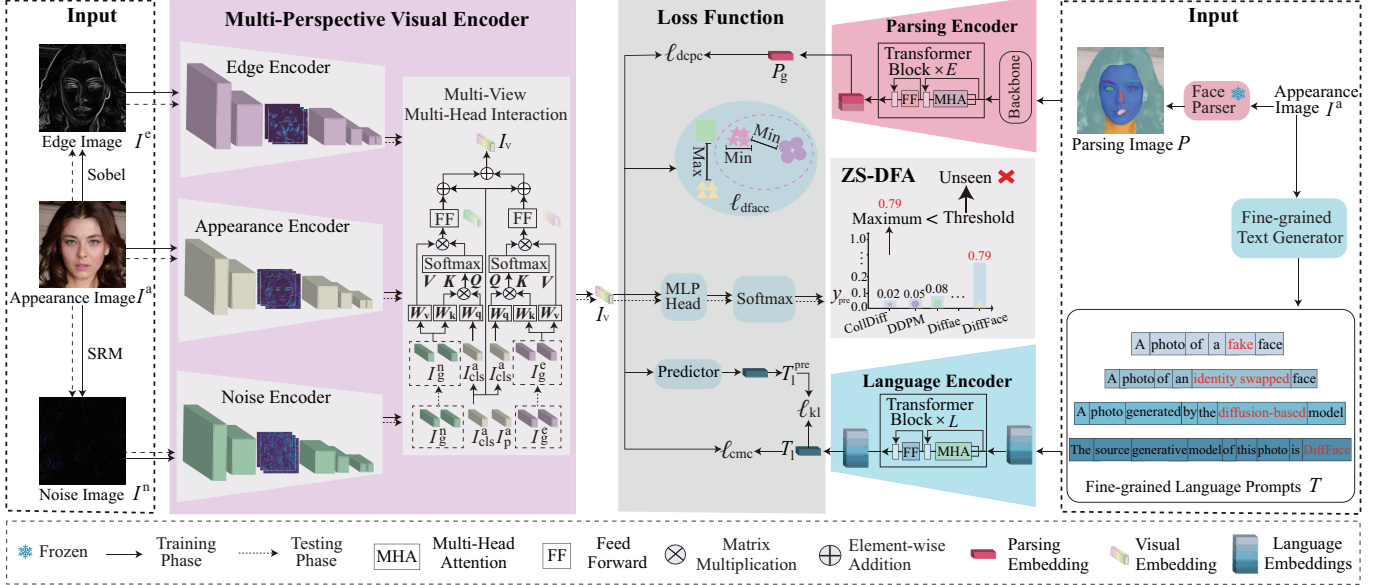


Fig. 3. The workflow of our PVLM model to conduct ZS-DFA. We first send the appearance image to the Sobel, SRM operator, and fine-grained text generator, to derive the edge image, noise image, parsing image, and text prompts, respectively. We then fed the appearance, edge, and noise image into MPVE to extract visual deepfake attribution features across multiple views. Meanwhile, the face parsing image and text prompts are transferred to the PE and LE to acquire face attribute features and language embeddings, accordingly. We then conduct the vision-language matching, dynamic vision-parsing alignment, and flexible metric learning. Finally, multi-view visual features are imparted to the MLP head and softmax to yield the prediction.

and patch token $I_p^a \in \mathbb{R}^{1 \times d}$ via disentangling I_g^a . Both EE and NE have similar architecture and workflow as AE. Given I^a , we employ the Sobel operator [20] to acquire edge images $I^e \in \mathbb{R}^{1 \times H \times W}$. We extract the richest image patch via the patch selector in [12] from I^a and then send them to the SRM [21] to gain the fine-grained noise image $I^n \in \mathbb{R}^{3 \times p \times p}$, where p denotes the size of the noise image. Like AE, EE and NE derive the global edge features $I_g^e \in \mathbb{R}^{2 \times d}$ and noise embeddings $I_g^n \in \mathbb{R}^{2 \times d}$, respectively.

Multi-view multi-head interaction module. First, to enhance the efficient interaction between noise and appearance features, we employ multi-head cross-attention (MHCA) between I_g^n and I_{cls}^a . Mathematically, the calculation of MHCA is as follows:

$$Q = I_{cls}^a W_q, \quad (1)$$

$$K = I_g^n W_k, \quad (2)$$

$$V = I_g^n W_v, \quad (3)$$

where $W_q, W_k, W_v \in \mathbb{R}^{d \times d_f}$, f denotes the number of head space, and $d_f = d/f$ is the dimension of feature tokens in the head space. To achieve global diverse fusion across noise and appearance representations, we devise the formula as follows:

$$MHCA(I_{cls}^a, I_g^n) = \text{softmax}\left(\frac{QK^T}{\sqrt{d_f}}\right)V. \quad (4)$$

Thereafter, the output of MHCA is projected and added to I_{cls}^a to get $I_{cls}^{an} \in \mathbb{R}^{1 \times d}$. The interaction between I_g^e and I_{cls}^a follows the same workflow as that between I_g^n and I_{cls}^a . Therefore, we can gain diverse and rich fusion features $I_{cls}^{ae} \in$

$\mathbb{R}^{1 \times d}$ across appearance and edge views. Finally, we boost the communication between I_{cls}^{an} and I_{cls}^{ae} to yield visual attribution features across three views.

$$I_v = I_{cls}^{an} + I_{cls}^{ae}. \quad (5)$$

D. Parsing Encoder

Different from current deepfake detection [24], [22], [25], [26], [27], [28] or DFA methods [7], [5] that tend to introduce discriminative prior knowledge like identity, landmark, or frequency features, we focus on the face parsing information since the source face attributes in fake images tend to be incompletely preserved [3]. As Fig. 2 shows, considering that there are evident source face attributes preservation differences between GAN and diffusion face images, GAN face images retain more source face attributes information than diffusion-generated ones. We aim to utilize the discriminative face parsing forgery patterns as prior information to facilitate DFA.

To align face parsing forgery features with multi-view visual ones and adapt face parsing information to our DFA domain, we design the parsing encoder (PE) consisting of a parsing backbone with stacked convolutional layers and a parsing transformer encoder (PTE) with E transformer blocks, TB_j^p , $j = 1, 2, \dots, E$, to capture global and diverse face parsing forgery representations. As shown in Fig. 3, given I^a , we use the CelebA-HQ pre-trained face parser [10] to generate the parsing image $P \in \mathbb{R}^{3 \times H \times W}$. Considering that the face parser may not accurately extract the parsing information of unseen faces, due to the domain gap between the pre-trained face dataset and the unseen one, we propose to conduct the parsing-guided multi-view DFA representation learning only during

training. Specifically, PE derives the local face parsing feature $P_{\text{loc}} \in \mathbb{R}^{c \times h \times w}$ from P through the backbone, to conduct the feature alignment. PE then imparts it to PTE to explore diverse long-range relations among features. In detail, P_{loc} is appended with a learnable class token to capture the global parsing attribution features, to obtain $P_{\text{tok}} = \text{App}(\text{Proj}(\text{Flat}(P_{\text{loc}}))) \in \mathbb{R}^{(n+1) \times d}$, where $n = \frac{chw}{chw}$ denotes the number of the parsing feature token sequence. It is then added with learnable position representations $P_e \in \mathbb{R}^{(n+1) \times d}$ to encode the position information, i.e.,

$$P_1^{\text{tra}} = P_{\text{tok}} \oplus P_e. \quad (6)$$

Subsequently, it is consecutively fed into E blocks, i.e.,

$$\begin{aligned} \text{PTE}(p_1^{\text{tra}}) &= \text{TB}_E^p \circ \text{TB}_{E-1}^p \circ \cdots \circ \text{TB}_2^p \circ \text{TB}_1^p(P_1^{\text{tra}}) \\ &= \text{TB}_E^p \circ \text{TB}_{E-1}^p \circ \cdots \circ \text{TB}_2^p(P_2^{\text{tra}}) \\ &= \cdots = \text{TB}_E^p \circ \text{TB}_{E-1}^p(P_{E-1}^{\text{tra}}) \\ &= \text{TB}_E^p(P_E^{\text{tra}}) = p_{\text{PTE}}^p, \end{aligned} \quad (7)$$

where \circ represents the function decomposition. PE derives global parsing attribution embeddings $P_g \in \mathbb{R}^{1 \times d}$ using the class token in P_{PTE}^p . To perform parsing-aware multi-view visual representation learning, we achieve the flexible vision-parsing matching via the proposed dynamic cross-perspective contrastive (DCPC) loss (See Sect. III-F).

E. Language Encoder

To create fine and accurate text attribution prompts, we introduce the fine-grained text generator (FTG) [12]. FTG generates text prompts for each image based on hierarchical fine-grained labels provided by the GenFace dataset. To prevent information leakage from texts and considering that unseen generators may lack text prompts, we introduce fine-grained texts to train our model only during training, to conduct language-guided multi-view representation learning. Specifically, given I^a , we generate deepfake attribution prompts T via FTG. To extract fine-grained language attribution-aware embeddings, we design the LE. As Fig. 3 shows, LE contains a language transformer encoder with L transformer blocks, TB_j^l , $j = 1, 2, \dots, L$. In detail, given the fine-grained deepfake attribution prompts T , LE first yields a series of word tokens $T^{\text{tok}} \in \mathbb{R}^t$ using the tokenizer [9], where t represents the number of word tokens. They are then projected to the word embedding vector $T^{\text{emb}} \in \mathbb{R}^{t \times d}$, and added with learnable position embeddings $P_l \in \mathbb{R}^{t \times d}$, i.e., $T_1^{\text{tra}} = T^{\text{emb}} + P_l$. Thereafter, they are consecutively transferred to L blocks, i.e.,

$$\begin{aligned} \text{LE}(T_1^{\text{tra}}) &= \text{TB}_L^l \circ \text{TB}_{L-1}^l \circ \cdots \circ \text{TB}_2^l \circ \text{TB}_1^l(T_1^{\text{tra}}) \\ &= \text{TB}_L^l \circ \text{TB}_{L-1}^l \circ \cdots \circ \text{TB}_2^l(T_2^{\text{tra}}) \\ &= \cdots = \text{TB}_L^l \circ \text{TB}_{L-1}^l(T_{L-1}^{\text{tra}}) \\ &= \text{TB}_L^l(T_L^{\text{tra}}) = T_{\text{LE}}^l. \end{aligned} \quad (8)$$

LE obtains the global deepfake attribution-perceptual language representations $T_l \in \mathbb{R}^{1 \times d}$ using the class token in T_{LE}^l , which are then employed for language-vision matching (See Sect. III-F).

F. Loss Function

Deepfake attribution loss. To capture discriminative DFA representations, we introduce the DFA loss as follows:

$$\mathcal{L}_{\text{dfa}} = \frac{1}{b} \sum_{u=1}^b -(y^u)^T \log(y_{\text{pre}}^u), \quad (9)$$

where $y_{\text{pre}} \in \mathbb{R}^x$, x is the number of the deepfake generators, b denotes the number of samples in a batch, and $u \in b$ is the index of samples.

Deepfake attribution contrastive center loss. However, learned DFA features are not general enough since the DFA loss merely considers the decision boundary among generators, rather than intra-generator compression and inter-generator separability. To address the limitation, we propose a novel DFACC loss. Unlike vanilla contrastive center (VCC) loss [13] which makes intra-generator samples closer and inter-generator ones farther apart, our DFACC loss minimizes the distance among within-generator samples, while placing correlated samples across generators closer and uncorrelated ones stay away from each other. In detail, our DFACC criterion is defined as:

$$\mathcal{L}_{\text{dfacc}} = \mathcal{L}_{\text{intra}} + \lambda \mathcal{L}_{\text{inter}}. \quad (10)$$

To achieve the intra-generator compaction, we design the $\mathcal{L}_{\text{intra}}$ loss as follows:

$$\mathcal{L}_{\text{intra}} = \frac{1}{b} \sum_{u=1}^b \|y_{\text{pre}}^u - c_{y^u}\|_2, \quad (11)$$

where $c_{y^u} \in \mathbb{R}^d$ denotes the trainable center vector of the generator y^u , $\|\cdot\|_2$ is the Euclidean distance, λ is the factor to balance the loss term, and y^u denotes the generator-specific one-hot label of the sample u . To minimize the distance among relevant samples across generators, and maximize the distance among unrelated ones, we propose the $\mathcal{L}_{\text{inter}}$ loss,

$$\mathcal{L}_{\text{inter}} = \frac{2}{b(b-1)} \sum_{u=1}^b \sum_{v=u+1}^b \mathbb{I}(y^u \neq y^v) \mathcal{L}_{uv}, \quad (12)$$

$$\mathbb{I}(y^u \neq y^v) = \begin{cases} 1, & \text{if } y^u \neq y^v, \\ 0, & \text{if } y^u = y^v, \end{cases} \quad (13)$$

$$\mathcal{L}_{uv} = \begin{cases} \max(\|y_{\text{pre}}^u - y_{\text{pre}}^v\|_2 - m, 0), & \text{if } \|c_{y^u} - c_{y^v}\|_2 < m, \\ -\|y_{\text{pre}}^u - y_{\text{pre}}^v\|_2, & \text{if } \|c_{y^u} - c_{y^v}\|_2 \geq m, \end{cases} \quad (14)$$

where m is a predefined margin threshold to control the interval among samples, \mathbb{I} is the indicator function, and $u, v = 1, 2, \dots, b$ is the sample index.

Dynamic cross-perspective contrastive loss. To achieve the flexible vision-parsing matching, we devise the DCPC loss. Mathematically, for the vision-parsing feature pairs $\{(I_v^u, P_g^u)\}_{u=1}^b$, we calculate the vision-parsing cosine similarity vector and the parsing-vision one as follows:

TABLE I

ZS-DFA EVALUATION ON PROTOCOL-1. ACC SCORES (%) ON UNSEEN GENERATORS, AFTER TRAINING USING SEEN GENERATORS. FORADAPTER IS FORENSICSADAPTER [29]. **BOLD** AND UNDERLINE DENOTE THE BEST AND THE SECOND-BEST RESULTS.

Methods	SimSwap	InSwapper	UniFace	e4s	VQGAN	SD-2.1	DiT	SiT	REFace	Average										
	Thr 0.7	Thr 0.9																		
CLIP [9]	9.12	17.44	<u>20.16</u>	28.08	18.24	28.56	37.60	<u>59.52</u>	7.20	10.72	19.52	36.32	10.48	17.76	14.40	23.28	64.88	77.76	22.40	33.27
CVIT [23]	11.76	25.04	8.08	20.08	13.44	27.04	26.72	48.00	25.76	47.04	15.84	34.08	21.52	39.52	20.24	37.44	15.04	31.92	17.60	34.46
CAEL [11]	3.36	6.56	5.04	9.52	5.44	9.60	20.48	43.04	0.80	1.92	36.56	61.44	1.92	5.44	2.64	6.56	23.28	49.12	11.06	21.46
MFCLIP [12]	21.36	46.72	13.76	31.12	20.40	44.96	29.76	57.04	14.88	35.76	12.72	26.16	13.52	30.16	10.64	27.12	25.92	49.28	18.11	38.70
DNA-Det	6.04	16.72	4.20	10.2	3.04	10.16	28.76	59.28	<u>29.08</u>	58.64	11.52	27.20	25.32	49.96	21.88	44.12	33.20	62.36	18.12	32.63
CPL [6]	<u>22.81</u>	<u>67.90</u>	14.54	42.60	<u>22.67</u>	<u>56.82</u>	<u>30.48</u>	60.04	30.80	61.92	13.74	38.44	26.92	<u>65.40</u>	22.70	<u>66.82</u>	35.28	63.12	<u>26.68</u>	<u>58.12</u>
CARZero [16]	2.21	3.82	2.07	3.73	2.43	3.71	9.36	17.04	3.61	6.92	7.91	17.44	2.03	3.59	3.01	5.37	9.36	20.05	4.67	9.07
DE-FAKE [4]	0.48	1.36	0.48	1.52	0.96	2.64	7.12	15.36	2.00	5.52	6.96	15.76	0.72	2.24	1.28	3.04	8.24	19.44	3.14	7.43
ForAdapter [29]	13.20	32.08	11.20	22.72	15.12	33.12	8.72	20.80	5.20	11.76	22.80	43.84	13.52	30.72	13.84	31.36	14.88	31.04	13.16	28.60
Ours	26.32	69.05	44.16	83.72	26.05	66.98	12.41	36.72	26.59	68.54	23.70	47.02	42.94	80.72	41.79	81.13	37.16	64.02	31.24	66.43

$$S_{v2p}^{uv}(I_v, P_g) = \frac{\exp(C(I_v^u, P_g^v)/\tau)}{\sum_{v=1}^b \exp(C(I_v^u, P_g^v)/\tau)} \odot \sigma(A^{uv}), \quad (15)$$

$$S_{p2v}^{uv}(P_g, I_v) = \frac{\exp(C(P_g^u, I_v^v)/\tau)}{\sum_{v=1}^b \exp(C(P_g^u, I_v^v)/\tau)} \odot \sigma(A^{uv}), \quad (16)$$

where τ is a learnable temperature weight to smooth features, $C(\cdot)$ executes a dot product operation to compute similarity scores, σ is a sigmoid function, $A \in \mathbb{R}^{b \times b}$ is a learnable weight matrix, \odot is a element-wise product, and $u, v = 1, 2, \dots, b$ are the index of the sample. The one-hot label y_{pa} of the u -th pair is denoted as $y_{pa}^u = \{y_{pa}^{uv}\}_{v=1}^b$, $y_{pa}^{uu} = 1$, $y_{pa}^{uv, u \neq v} = 0$. To pull positive pairs together, while pushing negative ones away, the DCPC loss is defined as:

$$\mathcal{L}_{dcpc} = \frac{1}{b} \left(- \sum_{u=1}^b (y_{pa}^u)^T [\log(S_{v2v}^u) + \log(S_{p2v}^u)] \right). \quad (17)$$

Like [12], we introduce the cross-modal contrastive (CMC) loss to perform vision-language matching, and the Kullback-Leibler (KL) divergence loss to conduct the feature alignment. The total loss is as follows:

$$\mathcal{L}_{\text{total}} = \mathcal{L}_{dfa} + \mathcal{L}_{dfacc} + \mathcal{L}_{cmc} + \mathcal{L}_{dcpc} + \mathcal{L}_{kl}. \quad (18)$$

IV. EXPERIMENTS

A. Experiment Setup

Dataset collection and protocol. We collect real and fake face images created by various advanced generators, including GAN and diffusion, based on several datasets, such as GenFace [11], DF40 [30], CelebAHQ [31], and FFHQ [32]. These fake data mainly involve three manipulations, including entire face synthesis (EFS), attribute manipulation (AM), and face swap (FS). Each forgery contains some GAN-based or diffusion-based generators. We define two protocols to evaluate the attribution performance of various models under zero-shot scenarios: 1) **Protocol-1** intends to investigate the performance of different attributors on unseen generators. It consists of 19 generators, such as GAN-based and diffusion-based ones from both the GenFace and DF40 datasets. We also generate the 2k fake faces using the CelebA-HQ pre-trained

TABLE II
THE OUTLINE OF THE DATASET CONSTRUCTION AND PROTOCOL. # DENOTES THE NUMBER OF DATASET. PRO MEANS THE PROTOCOL.

Seen Sets	Unseen Sets	Type	Sub-Type	Generator	Train #	Test #	Pro-1	Pro-2
GenFace	-	EFS	GAN	StyleGAN2	10,000	1,250	✓	✓
GenFace	-	EFS	GAN	StyleGAN3	10,000	1,250	✓	✓
GenFace	-	EFS	Diffusion	LatDiff	10,000	1,250	✓	✓
GenFace	-	EFS	Diffusion	ColDiff	10,000	1,250	✓	✓
GenFace	-	EFS	Diffusion	DDPM	10,000	1,250	✓	✓
GenFace	-	FS	GAN	FSLSD	10,000	1,250	✓	✓
GenFace	-	FS	GAN	FaceSwapper	10,000	1,250	✓	✓
GenFace	-	FS	Diffusion	DiffFace	10,000	1,250	✓	✓
GenFace	-	AM	GAN	LatTrans	10,000	1,250	✓	✓
GenFace	-	AM	Diffusion	Diffae	10,000	1,250	✓	✓
-	DF40	EFS	GAN	VQGAN	-	1,250	✓	✓
-	DF40	EFS	Diffusion	SD-2.1	-	1,250	✓	✓
-	DF40	EFS	Diffusion	DiT	-	1,250	✓	✓
-	DF40	FS	GAN	SimSwap	-	1,250	✓	✓
-	DF40	FS	GAN	UniFace	-	1,250	✓	✓
-	DF40	FS	GAN	InSwapper	-	1,250	✓	✓
-	DF40	FS	GAN	e4s	-	1,250	✓	✓
-	-	FS	Diffusion	REFace	-	1,250	✓	✓
CelebAHQ	-	Real	-	-	10,000	1,250	✗	✓
-	FFHQ	Real	-	-	-	1,250	✗	✓

REFace model [33], which is a diffusion-based FS method.

2) **Protocol-2** introduces additional original faces from both CelebA-HQ and FFHQ datasets based upon protocol-1.

Evaluation metrics. We leverage accuracy (ACC) as our evaluation metric. For zero-shot settings, unlike previous methods [7], [6] like OW-DFA that assign each novel deepfake to a specific category, considering that the categories of real-world generators are unknown and the goal of ZS-DFA is to identify generators beyond predefined categories, our approach groups all novel generators into a single unseen class. As shown in Fig. 3, like [34], [35], we obtain the maximum confidence score from logits yielded by the softmax function, and define a threshold to evaluate whether the model has encountered the generator or not. We label the generator as unseen when the maximum falls below the threshold. The higher the confidence score, the more confident the deepfake attributor is that it has encountered the generator. The higher threshold means that the model exhibits greater confidence in correct classification. We set the threshold to 0.7 and 0.9, respectively, and only report results for the threshold of 0.9 on protocol-1 in the ablation study. We chose the threshold to 0.7 since it implies a fairly strong prediction but still leaves room for some uncertainty, which helps avoid being too strict

TABLE III

ZS-DFA EVALUATION ON PROTOCOL-2. ACC SCORES (%) ON UNSEEN GENERATORS AND FFHQ, AFTER TRAINING USING SEEN GENERATORS AND CELEBA-HQ. **BOLD** AND UNDERLINE DENOTE THE BEST AND THE SECOND-BEST RESULTS.

Methods	SimSwap	InSwapper	UniFace	e4s	VQGAN	SD-2.1	DiT	SiT	REFace	FFHQ	Average
	Thr 0.7	Thr 0.9	Thr 0.7								
CLIP [9]	16.80	21.92	19.12	27.04	14.88	21.20	40.56	62.80	12.16	15.36	24.64
CViT [23]	28.24	49.04	19.44	39.04	29.84	50.00	21.20	37.04	16.16	31.52	17.60
CAEL [11]	4.88	12.24	8.96	21.6	6.96	18.00	33.12	<u>65.36</u>	18.40	36.64	31.92
MFCLIP [12]	33.68	63.20	35.28	64.16	34.08	63.84	24.96	50.48	<u>34.72</u>	63.12	11.76
DNA-Det [5]	27.56	61.60	26.28	63.84	18.20	50.16	<u>39.48</u>	77.56	26.32	50.00	19.84
CPL [6]	<u>35.70</u>	68.38	37.03	75.77	<u>36.26</u>	75.49	28.55	62.06	35.69	74.58	12.65
CARZero [16]	3.04	4.90	2.76	3.49	2.54	3.09	10.43	20.44	3.73	7.21	6.19
DE-FAKE [4]	1.12	2.32	1.36	2.88	1.20	2.48	8.56	19.84	2.40	5.12	5.92
ForAdapter [29]	12.48	30.00	16.88	33.60	15.04	33.68	21.60	45.20	1.76	5.04	16.56
Ours	36.89	72.05	54.71	87.62	39.07	<u>72.53</u>	17.95	40.84	34.51	73.68	30.91

and missing out on potentially useful classifications. We set the threshold to 0.9 because it denotes a very high level of confidence in the classification, and reduces the chance of misclassifications.

Implementation details. We implement the model using PyTorch on a Tesla V100 GPU with 32GB of memory under the Linux operating system. The number of transformer blocks E and L in PVLM are set to 6. The patch size p , feature dimension d , the factor λ , and batch size b are set to 112, 512, 0.5, and 32, respectively. The number of transformer blocks in AE, EE, and NE are set to 6, 3, and 3, respectively. We set the channel c , height h , and width w of feature maps to 512, 7, and 7, respectively. The height H and width W of images are configured to 224. We set the number t of word tokens to 308. Our method is trained with the Adam optimizer [36] using a learning rate of 1e-4 and a weight decay of 1e-3. We leverage the scheduler to drop the learning rate by ten times every 15 epochs. We conduct the normalization by dividing the image pixel values by 255, without any data augmentation operations. To ensure a fair comparison, we develop the SOTA methods using the codes provided by the authors and follow the default configurations, until convergence. All models are trained and evaluated using the same dataset protocols.

B. Comparison with the State of the Art

We evaluate state-of-the-art methods on our benchmark dataset. We select various deepfake attributors such as hybrid transformer-based (i.e., CViT [23] and CAEL [11]), vision-language-based (i.e., CLIP [9], MFCLIP [12], and ForensicsAdapter [29]), zero-shot learning-based (CARZero [16]), and methods dedicated to attributing deepfake images (e.g., DNA-Det [5], CPL [6], and DE-FAKE [4]).

Results on protocol-1. To study the attribution performance of different models, we conduct the ZS-DFA evaluation using protocol-1. We test models on various unseen generators from DF40 after training using seen generators from GenFace. In Table I, our method exceeds most attributors by a wide gap. It also surpasses the recent network MFCLIP by about 13% ACC under the threshold of 0.7. Unlike MFCLIP which conducts the fine-grained language-guided image-noise forgery representation learning, our model introduces face parsing global features to conduct the bi-modality (e.g., text and parsing) guided multiple perspectives (e.g., image, noise, and edge)

DFA representation learning. Compared to the DFA methods, the ACC of our method is nearly 4% and 13% higher than that of CPL and DNA-Det, validating the effectiveness of our model. Unlike DNA-Det, which only explores global attribution features within the image modality via patch-based contrastive learning, our model focuses on multiple modalities, including text and face parsing, as well as multiple views, such as image, noise, and edge, to achieve predominant ZS-DFA. Besides, the ACC score of models using the threshold of 0.9 is higher than that of models using the threshold of 0.7, which validates the reliability and effectiveness of the chosen threshold. We argue that a higher threshold necessitates that the model exhibit greater confidence in correct classification, thereby reducing the occurrence of misclassifications.

Results on protocol-2. To further assess the attribution performance of various methods, we conduct the ZS-DFA evaluation on protocol-2. We test models on various unseen generators and FFHQ after training using both seen generators and CelebA-HQ. In Table III, the ACC of our method exceeds that of most SOTAs, showing the superior ZS-DFA capability of our method. Specifically, the average ACC score of our PVLM model is about 19.31% higher than that of CViT on protocol-2. Unlike CViT merely explores global image forgery traces, our method focuses on global visual forgery features across three views (i.e., image, noise, and edge) and conducts fine-grained vision-language alignment and vision-parsing matching. Besides, models trained using protocol-2 outperform those trained with protocol-1. For instance, MFCLP and DNA-Det gain the average ACC score of 38.70% and 32.63% under the threshold of 0.9 setting on protocol-1, respectively. By contrast, they attain 43.38% and 50.48% ACC on protocol-2. It is noticed that a nearly 4.7% and 17.85% growth of ACC could be realized by adding original face distributions, which shows that pristine face images could facilitate the ZS-DFA performance of various deepfake attributors. We argue that models may extract more discriminative and common forgery features for each generator, due to the addition of authentic face distributions.

Generalization to unseen in-the-wild deepfake datasets. To offer stronger evidence of domain robustness beyond synthetic benchmarks, we train networks using protocol-2 and test them on unseen in-the-wild deepfake datasets, such as WildDeepfake [37], Celeb-DF [38], and DFDC [39]. In

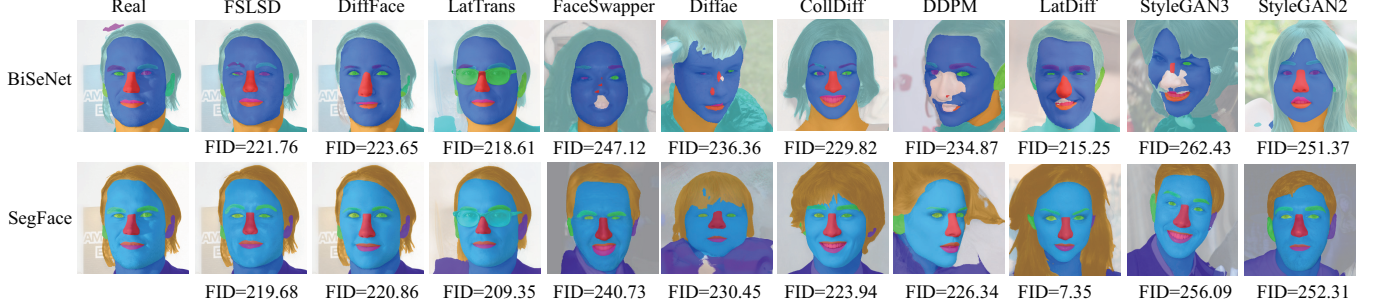


Fig. 4. Visualization of parsing images produced by different face parsers for fake images synthesized by various generators.

TABLE IV

ZS-DFA EVALUATION ON UNSEEN IN-THE-WILD DEEPFAKE DATASETS.
ACC SCORES (%) ON UNSEEN DEEPFAKE DATASETS, AFTER TRAINING
USING SEEN GENERATORS AND CELEBA-HQ.

Methods	Celeb-DF		DFDC		WildDeepfake		Average		Params Thr 0.7 Thr 0.9 Thr 0.7 Thr 0.9 Thr 0.7 Thr 0.9 Thr 0.7 Thr 0.9	Inference Time (s)
	Thr 0.7	Thr 0.9								
CLIP [9]	2.56	8.56	8.64	17.92	17.68	39.52	9.63	22.00	84.23	1.41
CViT [23]	7.28	14.24	25.84	47.36	19.84	43.20	17.65	34.93	89.02	0.26
CAEL [11]	12.96	28.32	9.52	23.44	21.76	49.52	14.75	33.76	158.63	3.74
MFCLIP [12]	34.88	62.32	28.48	58.16	29.68	60.64	31.01	60.37	93.83	1.67
DNA-Det [5]	17.12	41.36	25.04	48.08	0.90	3.28	14.35	30.91	6.23	0.13
CPL [6]	35.06	64.24	29.50	57.32	24.91	56.02	29.82	59.19	10.79	0.17
CARZero [16]	7.86	12.65	8.09	10.64	9.37	25.90	8.44	16.36	84.24	1.42
DE-FAKE [4]	4.16	9.92	2.08	4.4	7.04	14.64	4.43	9.65	84.24	1.42
ForAdapter[29]	11.36	27.60	20.48	47.44	25.36	56.08	19.07	43.71	5.70	0.57
Ours	36.14	68.24	27.78	60.75	31.28	68.56	31.73	65.85	242.25	0.11

Table IV, our model surpasses most methods across various fake face images from unseen datasets, which shows that our model achieves excellent domain robustness. To conduct the runtime benchmark, we assess the computational costs of models, including the parameter count and inference time. Although our PVLM model has a larger number of parameters than the lightweight DNA-Det, the attribution performance of PVLM is significantly improved on unseen deepfake datasets. In particular, the ACC score of PVLM is about 30% higher than that of DNA-Det, with an increase of 236.02M parameters but a reduction of 0.02s in the inference time. In the future, we aim to apply knowledge distillation and model architecture modifications, such as a window-based multi-head self-attention, to achieve faster efficiency.

Robustness to unseen image corruptions. We evaluate the robustness of deepfake attributors against various unseen image perturbations. We train networks using protocol-2, and test their ZS-DFA performance on unseen distorted images from [40]. Ten types of corruption are engaged, each with five severity levels. As Fig. 5 displays, we test attributors on diverse image distortions, including saturation changes, contrast adjustments, block distortions, white Gaussian noise, blurring, pixelation, video compression, upscaling, downscaling, and cropping. A severity of 0 means no corruption. Specifically, the specific settings for the severity of the seven deformations are discussed in detail in [12]. In Fig. 5, we notice that the ACC of networks tend to decrease with the growth of downscaling severities. By contrast, the ACC of our PVLM method shows a rising trend, verifying the strong attribution robustness of

PVLM. Furthermore, the results demonstrate that our model outperforms most existing methods across different types of image degradation.

C. Ablation Study

We conduct ablation study including impacts of various modules, the face parser, various losses, the fine-grained text prompts, the MMI module, the margin or factor in DFACC loss.

Effects of various modules. To evaluate the contribution of each module to learning ability, we observe the DFA performance on both seen and unseen generators using protocol 1. In Table VII, NE improves the performance of the attributor by 2.34% ACC on images created by unseen generators, showing that SRM noises provide significant clues to facilitate ZS-DFA. The improvement from incorporating EE (+2.48%) is clear, highlighting the importance of edge global embeddings. LE further boosts performance by about 21% ACC, when EE or PE is also involved. The gain brought by LE alone is marginal without the integration of EE or PE, as the effectiveness of LE relies on the synergy between the different features. LE provides fine-grained semantic guidance, which is enhanced when combined with the distinctive facial parsing prior information from PE or edge features from EE. Without these modules, LE's potential is not fully realized, leading to a smaller performance gain. Besides, when the MPVE module (i.e. AE+NE+EE) is involved, the ACC of the model is 43.67% on unseen generators. The improvement from adding PE (+15.36%) is evident, highlighting the importance of discriminative facial parsing guidance. LE enhances performance by about 7.4% ACC on unseen generators. The combined gain from integrating both PE and LE (+22.76%) is particularly striking. We argue that fine-grained language embeddings from LE and facial attribute information from PE reinforce and enhance each other, synergistically guiding the model to capture both general and distinct attribution embeddings.

Impacts of the DFACC loss. Models are trained with the VCC loss and the DFACC loss, respectively. In Table V, the ACC of both CLIP and PVLM supervised by the VCC loss are 79.04% and 96.90% on protocol-1, respectively. By contrast, they achieve 89.07% ACC and 100% ACC under the constraints of our DFACC criteria, accordingly, which verifies the necessity of conducting intra-generator compactness and inter-generator separability based on the correlation among generators. We

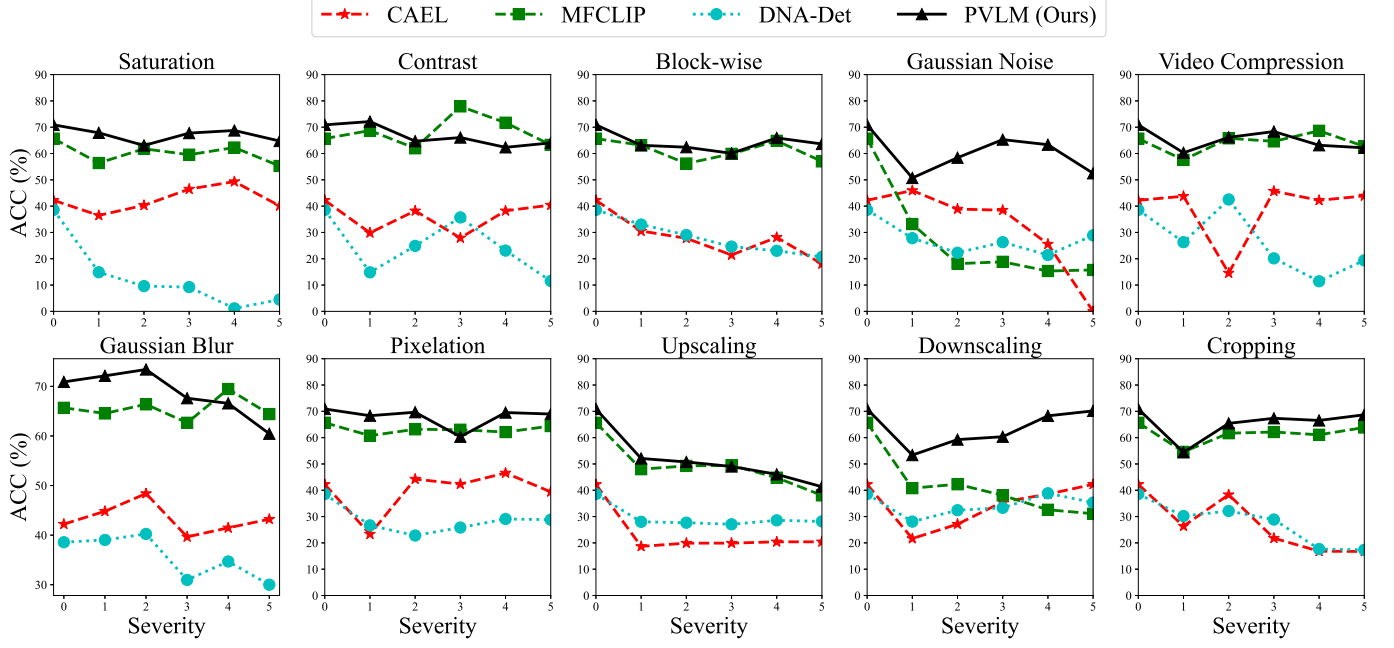


Fig. 5. Robustness to unknown image deformations.

TABLE V
EFFECTS OF DIFFERENT
CONTRASTIVE CENTER LOSSES.

Method	Protocol-1	
	Seen	Unseen
	ACC	ACC
CLIP w/VCC	79.04	-
CLIP w/DFACC	89.07	-
Ours w/VCC	96.90	62.88
Ours w/DFACC	100	66.43

TABLE VI
EFFECTS OF VARIOUS FACE
PARSERS.

Method	Protocol-1	
	Seen	Unseen
	ACC	ACC
SegFace w/ConNet	96.40	47.09
SegFace w/ResNet	97.80	59.35
SegFace w/Swin-B	96.92	48.90
BiSeNet	100	66.43

TABLE VII
MODEL ABLATION. ACC SCORES (%) ON PROTOCOL-1.

AE	NE	EE	PE	LE	Model	
					Seen	Unseen
✓					99.58	34.46
		✓			99.83	29.71
	✓				99.66	23.97
✓	✓				99.72	36.80
✓	✓			✓	100	38.70
✓	✓		✓	✓	100	61.64
✓	✓	✓			99.99	34.62
✓	✓	✓			99.80	43.67
✓	✓	✓	✓		99.92	59.03
✓	✓	✓	✓	✓	100	61.25
✓	✓	✓	✓	✓	100	66.43

visualize features extracted from samples produced by various generators using t-SNE [41]. We randomly select 500 samples for each seen generator from the testing set of protocol-1. In Fig. 6, samples of each generator are clustered in respective domains. With the addition of the DFACC loss, samples within the generator are more compact, with those of highly correlated generators aggregated and those of weakly related ones

separated. This shows that our DFACC loss realizes flexible intra-generator aggregation and inter-generator separation.

Influences of the face parser. We delve into the impact of various face parsers, such as SegFace [42] and BiSeNet [10]. We test frameworks on protocol-1. In Table VI, the ACC reaches the maximum as the BiSeNet is involved. We argue that face parsing images extracted by BiSeNet are more discriminative than those encoded by other face parsers, which could boost DFA. We visualize parsing images generated by various face parsers, such as BiSeNet and SegFace, for fake faces produced by various generators. In Fig. 4, compared to SegFace, the BiSeNet face parser does not generalize well to unseen diffusion faces. There are more evident distinctions among various generator parsing images produced by BiSeNet, visually. We attribute this to BiSeNet’s design as a lightweight face parsing network, optimized for real-world data. Unlike more complex models, such as GAN-based architectures or vision transformers like SegFace, BiSeNet may lack the capacity and flexibility to handle the unique characteristics of generative models and may also struggle with the high-frequency details and artifacts typical of diffusion models.

We further calculate the FID score of the various generator parsing images created by different face parsers. To ensure a fair and balanced evaluation, we maintain an equal distribution of genuine and forged face parsing images, at a 1:1 ratio. We use 10,000 real images and 10,000 fake images to calculate the FID score for each generator. Lower FID scores denote better image quality. Results across various generators are shown in Fig. 4. The FID score of diffusion parsing images from BiSeNet is higher than that of those from SegFace, showing that BiSeNet struggles to generalize to unseen diffusion faces. Despite the performance degradation of BiSeNet, in Table VI, the ACC score of the model with BiSeNet is higher than that of the model with SegFace. We argue that there are evident

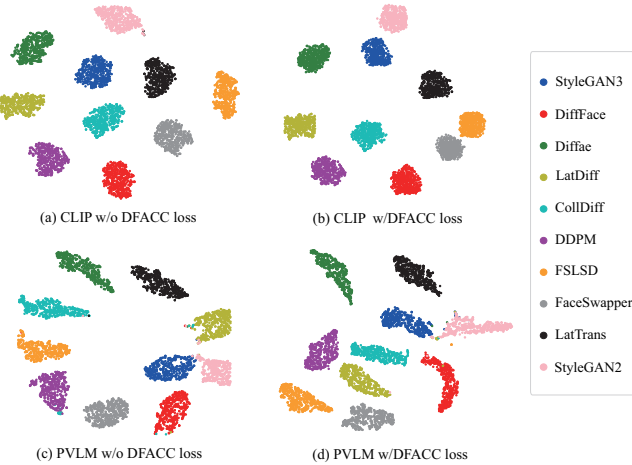


Fig. 6. The t-SNE visualization of various models (w/o or w/ DFACC loss).

distinctions among various generator parsing distributions produced by BiSeNet, which can facilitate DFA.

Impacts of different losses. To delve into the contribution of loss functions, we conduct ablations on different losses. The ablation result of various losses is displayed in Table X. When PVLM is supervised with purely DFA loss, the ACC is 35.76% on unseen generators, but an increase of about 4.4% in ACC could be achieved via adding the DFACC criterion. We argue that it could boost the generalizable deepfake attribution representations via flexible contrastive learning across various generators. At the same time, owing to the addition of the CMC loss, PVLM is improved by 20.05% ACC on unseen generators, demonstrating the effectiveness of language guidance. The introduction of the DCPC loss further increases the performance (+5.5%), which shows that the global face parsing features could be valuable prior information for both deepfake detection and attribution. Moreover, due to the integration of the KL loss, our PVLM model achieves an enhancement of 0.7% ACC, which indicates that it is valuable to conduct feature alignment between visual and textual modalities. The incorporation of the five criteria yields the best performance among these losses, indicating that the proposed loss realizes promising results.

Effects of the margin m in DFACC loss. In the DFACC loss, we measure the correlation between generators based on the margin value. We investigate the influence of different margin values on model performance. As shown in Table XII, the ACC score tends to improve with an increase of the margin value, indicating that a larger margin enhances the model's ability to distinguish between generators, effectively. Notably, the performance reaches the peak when the margin value is set to 0.7. This suggests that a margin of 0.7 can serve as an optimal value for evaluating the correlation among generators.

Influences of the language encoder. To delve into the impact of LE, we conduct ablation experiments using protocol-1. The ablation results are shown in Table IX. The gains from introducing the LE module (+7.4%) are obvious. We argue that LE offers fine-grained and accurate language guidance via vision-language matching, which could enhance the DFA

TABLE VIII
EFFECTS OF TEXT PROMPTS. LP
IS THE LEARNABLE PROMPT.

Method	Protocol-1	
	Seen Unseen	
	ACC	ACC
CLIP w/LP	53.52	-
CLIP w/o LP	79.04	-
Ours w/ LP	82.58	45.79
Ours w/o LP	100	66.43

TABLE IX
EFFECTS OF THE LANGUAGE
ENCODER.

Method	Protocol-1	
	Seen Unseen	
	ACC	ACC
Ours w/o LE	99.92	59.03
Ours w/ LE	100	66.43

TABLE X
EFFECTS OF VARIOUS LOSSES.

Method	Protocol-1	
	Seen Unseen	
	ACC	ACC
\mathcal{L}_{dfa}	99.32	35.76
$\mathcal{L}_{dfa} + \mathcal{L}_{dfacc}$	99.74	40.16
$\mathcal{L}_{dfa} + \mathcal{L}_{dfacc} + \mathcal{L}_{cmc}$	99.98	60.21
$\mathcal{L}_{dfa} + \mathcal{L}_{dfacc} + \mathcal{L}_{cmc} + \mathcal{L}_{depc}$	100	65.73
$\mathcal{L}_{dfa} + \mathcal{L}_{dfacc} + \mathcal{L}_{cmc} + \mathcal{L}_{depc} + \mathcal{L}_{kl}$	100	66.43

performance of models.

Impacts of the MMI module. To study the effect of MMI, we conduct ablation experiments using protocol-1. The ablation results are shown in Table XI. The gains from adding the MMI module (+3.26%) are evident. We argue that MMI facilitates diverse and comprehensive multi-view interactions, promoting the model to extract rich attribution features.

Effects of the fine-grained text prompts. To study the impact of fine-grained text prompts on model performance, we introduce learnable prompts with insufficient accuracy, to train PVLM and CLIP, respectively. In Table VIII, the performance of both CLIP and PVLM declines significantly (-25.52% and -17.42%), due to the addition of learnable text prompts, accordingly. We argue that elaborate and accurate semantic guidance plays a vital role in fine-grained DFA tasks.

Influences of the factor λ in DFACC loss. In the DFACC loss, we define the factor λ to balance the loss term between \mathcal{L}_{intra} and \mathcal{L}_{inter} . We study the effect of various factors on model performance. As Table XIII displays, the ACC score rises with the increase of factors, which indicates the effectiveness of flexible metric learning. Specifically, the performance reaches its peak when the weight factor λ is set to 0.5, which means an optimal balance between the two loss terms. We argue that the optimal setting of λ allows the model to learn the most discriminative features, leading to better generalization and more accurate predictions.

V. VISUALIZATION

Visualization of confusion matrix. We visualize the confusion matrix to observe the predictions of different models. As shown in Fig. 8, MFCLIP achieves lower prediction results compared to PVLM. In detail, some samples may be misclassified, particularly in the following cases: when the data source is identical, such as StyleGAN2 and FSLSD, or when they can be categorized into the same classes, such as the diffusion-based model (e.g., DiffFace and Diffae). By contrast,

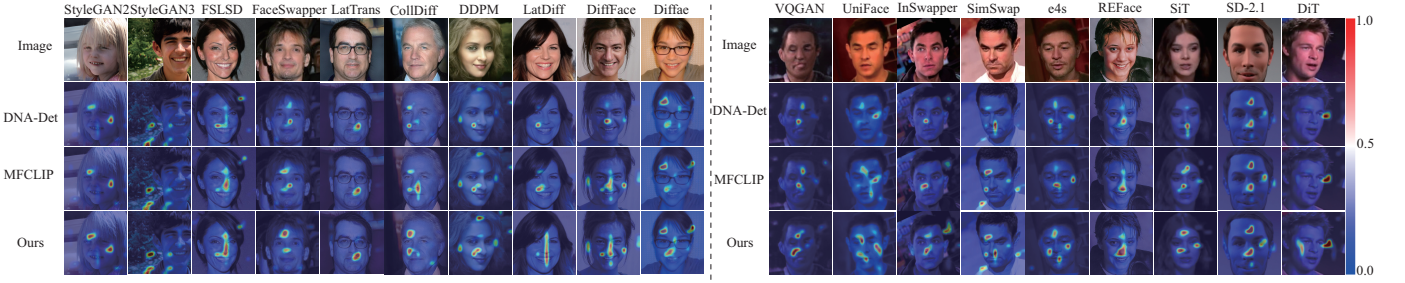


Fig. 7. The heatmap visualization of various models on the sample created by the seen (Left) or unseen (Right) generators. The hotter (red color) a position is, the more forgery traces are captured by the models.

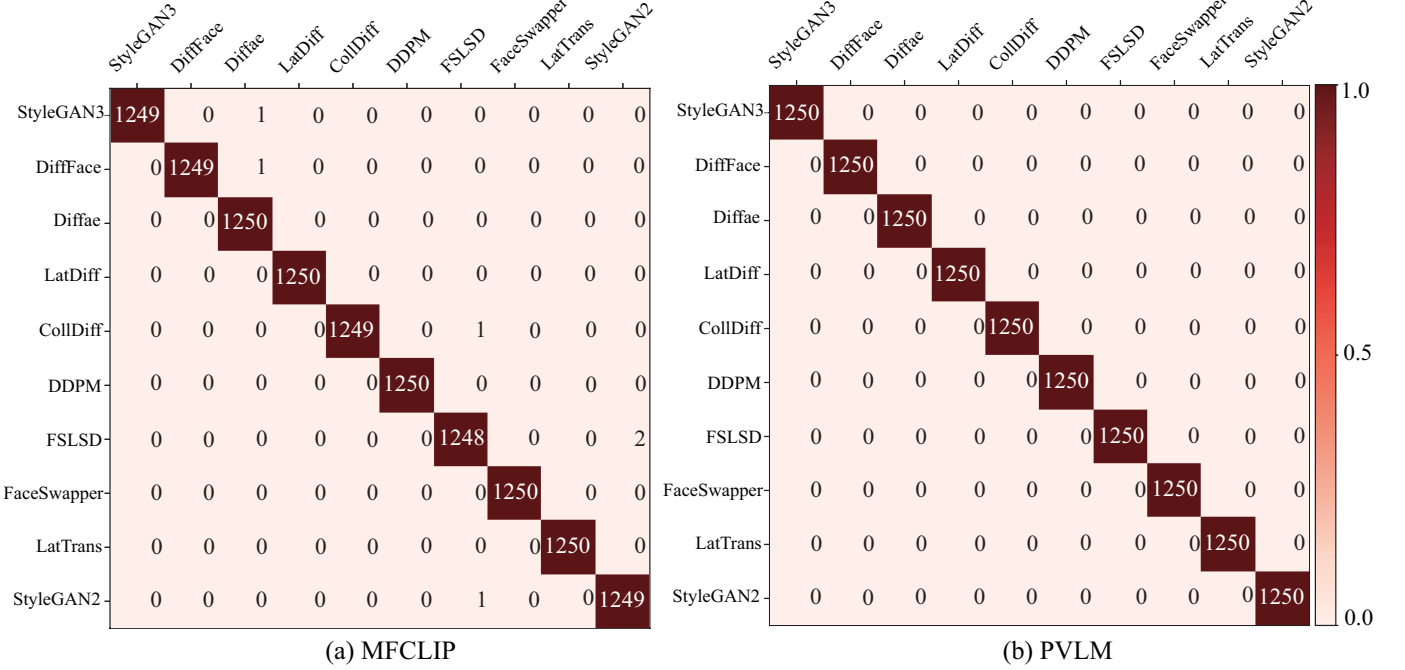


Fig. 8. Confusion matrix visualization of various methods. The darker red means more frequent or stronger predictions, and the lighter red denotes less frequent or weaker predictions.

TABLE XI
EFFECTS OF THE MMI MODULE.

Method	Protocol-1	
	Seen	Unseen
	ACC	ACC
Ours w/o MMI	99.60	63.17
Ours w/ MMI	100	66.43

our PVLM method is capable of decreasing confusion between similar generators while achieving more accurate predictions, i.e., 100% ACC on all generators.

Visualization of heatmaps. To enhance the interpretability of the proposed method, we visualize the heatmap yielded by various settings using the Grad-CAM [43]. In Fig. 7, we show the heatmap of samples generated by various seen and unseen generators for three models, respectively. Each column shows a fake face synthesized by different generators. The second to fourth rows display heatmaps for three DFA models: DNA-

TABLE XII
INFLUENCE OF MARGIN VALUES IN DFACC LOSS.

Method	Protocol-1	
	Seen	Unseen
	ACC	ACC
CLIP	m=0.5	88.85
	m=0.7	89.07
	m=0.9	79.01
PVLM (Ours)	m=0.5	98.02
	m=0.7	100
	m=0.9	99.40
		49.36
		66.43
		54.98

Det, MFCLIP, and our PVLM method. It is observed that PVLM mines more comprehensive forgery traces than both MFCLIP and DNA-Det. As shown in Fig. 7, attributors tend to identify forgery regions such as eyes, nose, and mouth. It is noted that DFA could be regarded as a fine-grained forgery detection task, since manipulated artifacts created by generators are prone to being subtle and faint.

TABLE XIII
INFLUENCE OF THE FACTOR IN DFACC LOSS.

Method	Testing Set		
	Seen	Unseen	
	ACC	ACC	
CLIP	$\lambda=0.0$	79.46	34.89
	$\lambda=0.3$	82.12	35.60
	$\lambda=0.5$	88.85	38.21
	$\lambda=0.7$	87.86	37.65
PVLM (Ours)	$\lambda=0.0$	94.37	62.24
	$\lambda=0.3$	97.46	64.02
	$\lambda=0.5$	100	66.43
	$\lambda=0.7$	98.03	64.28

TABLE XIV
ACC RESULTS (%) OF MODELS FOR DEEPFAKE DETECTION AND DEEPFAKE ATTRIBUTION ON PROTOCOL-2.

Method	Deepfake Detection		Deepfake Attribution	
	Seen	Unseen	Seen	Unseen
	ACC	ACC	ACC	ACC
CLIP [9]	73.56	63.08	82.72	35.98
CAEL [11]	99.63	83.09	99.83	30.86
MFCLIP [12]	99.74	86.49	99.91	43.38
DE-FAKE [4]	97.07	69.32	98.15	9.30
DNA-Det [5]	96.18	67.02	99.65	50.48
PVLM (Ours)	99.90	89.45	100	67.61

VI. DEEPFAKE DETECTION

To study the significance of DFA, we evaluate the performance of the deepfake detectors and the deepfake attributors model using Protocol-2, respectively. The results of models on two tasks (i.e., deepfake detection and deepfake attribution) are displayed in Table XIV. It is noticed that the classification tends to become easier, with the number of categories increasing from 2 (deepfake detection) to 11 (deepfake attribution). We argue that there is a growing distinction between pristine and forged images, as the number of categories rises, which facilitates deepfake detection. For example, MFCLIP and DNA-Det obtain 99.74% ACC and 96.18% ACC on seen generators under the deepfake detection setting, respectively. By contrast, they achieve 99.91% ACC (+0.17%) and 99.65% ACC (+2.47%) on seen generators in DFA tasks, accordingly.

VII. CONCLUSION

In this paper, we conduct a novel fine-grained ZS-DFA benchmark. Besides, we propose an innovative parsing-aware vision language model with dynamic contrastive learning (PVLM) method, which introduces face parsing modality to enhance the learning of visual forgery features across image, noise, and edge views, thus mining both general and discriminative attribution patterns, to achieve ZS-DFA. Although our method has achieved excellent ZS-DFA, the interaction among vision, parsing, and language modalities is limited. We intend to explore diverse and efficient vision-language-parsing communication mechanisms to improve the ZS-DFA performance of PVLM. We also plan to introduce abundant face data generated by various generators like flow-based and auto-regressive models, to facilitate ZS-DFA. We hope that

our new benchmark and PVLM model could provide new insights for the research direction, such as deepfake attribution, deepfake detection, and vision language model.

REFERENCES

- [1] I. Goodfellow, J. Pouget-Abadie, M. Mirza, B. Xu, D. Warde-Farley, S. Ozair, A. Courville, and Y. Bengio, “Generative Adversarial Nets,” in *Proceedings of the Advances in Neural Information Processing Systems (NIPS)*, 2014, pp. 2672–2680.
- [2] K. Kim, Y. Kim, S. Cho, J. Seo, J. Nam, K. Lee, S. Kim, and K. Lee, “DiffFace: Diffusion-based face swapping with facial guidance,” *arXiv preprint arXiv:2212.13344*, 2022.
- [3] G. Pei, J. Zhang, M. Hu, Z. Zhang, C. Wang, Y. Wu, G. Zhai, J. Yang, C. Shen, and D. Tao, “Deepfake generation and detection: A benchmark and survey,” *arXiv preprint arXiv:2403.17881*, 2024.
- [4] Z. Sha, Z. Li, N. Yu, and Y. Zhang, “De-fake: Detection and attribution of fake images generated by text-to-image generation models,” in *Proceedings of the ACM SIGSAC Conference on Computer and Communications Security*, 2023, p. 3418–3432.
- [5] T. Yang, Z. Huang, J. Cao, L. Li, and X. Li, “Deepfake network architecture attribution,” in *Proceedings of the AAAI Conference on Artificial Intelligence (AAAI)*, 2022, pp. 4662–4670.
- [6] Z. Sun, S. Chen, T. Yao, B. Yin, R. Yi, S. Ding, and L. Ma, “Contrastive pseudo learning for open-world deepfake attribution,” in *Proceedings of the IEEE International Conference on Computer Vision (ICCV)*, 2023, pp. 20825–20835.
- [7] Z. Sun, S. Chen, T. Yao, R. Yi, S. Ding, and L. Ma, “Rethinking open-world deepfake attribution with multi-perspective sensory learning,” *Int. J. Comput. Vision*, vol. 133, no. 2, p. 628–651, Aug. 2024.
- [8] H. Cheng, Y. Guo, T. Wang, L. Nie, and M. Kankanhalli, “Diffusion facial forgery detection,” in *Proceedings of the 32nd ACM International Conference on Multimedia (MM)*, 2024, p. 5939–5948.
- [9] A. Radford, J. W. Kim, C. Hallacy, A. Ramesh, G. Goh, S. Agarwal, G. Sastry, A. Askell, P. Mishkin, J. Clark *et al.*, “Learning transferable visual models from natural language supervision,” in *Proceedings of the International Conference on Machine Learning (ICML)*, 2021, pp. 8748–8763.
- [10] V. Yakhyokhuja, “face-parsing,” <https://github.com/zlrunning/face-parsing.PyTorch>, 2024.
- [11] Y. Zhang, Z. Yu, T. Wang, X. Huang, L. Shen, Z. Gao, and J. Ren, “Genface: A large-scale fine-grained face forgery benchmark and cross appearance-edge learning,” *IEEE Transactions on Information Forensics and Security*, vol. 19, pp. 8559–8572, 2024.
- [12] Y. Zhang, T. Wang, Z. Yu, Z. Gao, L. Shen, and S. Chen, “Mfclip: Multi-modal fine-grained clip for generalizable diffusion face forgery detection,” *IEEE Transactions on Information Forensics and Security*, vol. 20, pp. 5888–5903, 2025.
- [13] C. Qi and F. Su, “Contrastive-center loss for deep neural networks,” in *Proceedings of the IEEE International Conference on Image Processing (ICIP)*, September 2017, pp. 2851–2855.
- [14] S. Girish, S. Suri, S. S. Rambhatla, and A. Shrivastava, “Towards discovery and attribution of open-world gan generated images,” in *Proceedings of the IEEE international conference on computer vision (CVPR)*, 2021, pp. 14 094–14 103.
- [15] J. Shipard, A. Wiliem, K. N. Thanh, W. Xiang, and C. Fookes, “Diversity is definitely needed: Improving model-agnostic zero-shot classification via stable diffusion,” in *Proceedings of the IEEE Conference on Computer Vision and Pattern Recognition (CVPR)*, 2023, pp. 769–778.
- [16] H. Lai, Q. Yao, Z. Jiang, R. Wang, Z. He, X. Tao, and S. K. Zhou, “Carzero: Cross-attention alignment for radiology zero-shot classification,” in *Proceedings of the IEEE Conference on Computer Vision and Pattern Recognition (CVPR)*, 2024, pp. 11 137–11 146.
- [17] Y. Li, X. Hou, Z. Dezh, L. Shen, and Z. Zhao, “Flip-80m: 80 million visual-linguistic pairs for facial language-image pre-training,” in *Proceedings of the ACM International Conference on Multimedia (MM)*, 2024, p. 58–67.
- [18] Y. Kalantidis, G. Tolias *et al.*, “Label propagation for zero-shot classification with vision-language models,” in *Proceedings of the IEEE Conference on Computer Vision and Pattern Recognition (CVPR)*, 2024, pp. 23 209–23 218.
- [19] O. Saha, G. Van Horn, and S. Maji, “Improved zero-shot classification by adapting vlm with text descriptions,” in *Proceedings of the IEEE Conference on Computer Vision and Pattern Recognition (CVPR)*, 2024, pp. 17 542–17 552.

[20] N. Kanopoulos, N. Vasanthavada, and R. L. Baker, "Design of an image edge detection filter using the Sobel operator," *IEEE Journal of Solid-state Circuits*, vol. 23, no. 2, pp. 358–367, 1988.

[21] J. Fridrich and J. Kodovsky, "Rich models for steganalysis of digital images," *IEEE Transactions on Information Forensics and Security*, vol. 7, no. 3, pp. 868–882, 2012.

[22] C. Tan, Y. Zhao, S. Wei, G. Gu, P. Liu, and Y. Wei, "Frequency-aware deepfake detection: Improving generalizability through frequency space domain learning," in *Proceedings of the AAAI Conference on Artificial Intelligence (AAAI)*, vol. 38, no. 5, 2024, pp. 5052–5060.

[23] D. Wodajo and S. Atnafu, "Deepfake video detection using convolutional vision transformer," 2021, arXiv preprint arXiv:2102.11126.

[24] T. Wang, M. Huang, H. Cheng, X. Zhang, and Z. Shen, "Lampmark: Proactive deepfake detection via training-free landmark perceptual watermark," in *Proceedings of the ACM International Conference on Multimedia (MM)*, 2024, p. 10515–10524.

[25] Y. Zhang, Q. Li, Z. Yu, and L. Shen, "Distilled transformers with locally enhanced global representations for face forgery detection," *Pattern Recognition*, vol. 161, p. 111253, 2025.

[26] J. Deng, C. Lin, P. Hu, C. Shen, Q. Wang, Q. Li, and Q. Li, "Towards benchmarking and evaluating deepfake detection," *IEEE Transactions on Dependable and Secure Computing*, vol. 21, no. 6, pp. 5112–5127, 2024.

[27] J. Hu, J. Liang, Z. Qin, X. Liao, W. Zhou, and X. Lin, "Ada-finer: Inferring face representations from adaptive select frames for high-visual-quality deepfake detection," *IEEE Transactions on Dependable and Secure Computing*, vol. 22, no. 3, pp. 3011–3027, 2025.

[28] B. Zhang, Q. Yin, W. Lu, and X. Luo, "Deepfake detection and localization using multi-view inconsistency measurement," *IEEE Transactions on Dependable and Secure Computing*, vol. 22, no. 2, pp. 1796–1809, 2025.

[29] X. Cui, Y. Li, A. Luo, J. Zhou, and J. Dong, "Forensics adapter: Adapting clip for generalizable face forgery detection," in *Proceedings of the Computer Vision and Pattern Recognition Conference*, 2025, pp. 19207–19217.

[30] Z. Yan, T. Yao, S. Chen, Y. Zhao, X. Fu, J. Zhu, D. Luo, C. Wang, S. Ding, Y. Wu, and L. Yuan, "Df40: Toward next-generation deepfake detection," in *Proceedings of the Advances in Neural Information Processing Systems (NIPS)*, vol. 37, 2024, pp. 29387–29434.

[31] T. Karras, T. Aila, S. Laine, and J. Lehtinen, "Progressive growing of GANs for improved quality, stability, and variation," in *Proceedings of the International Conference on Learning Representations (ICLR)*, 2018, pp. 26–37.

[32] T. Karras, S. Laine, and T. Aila, "A style-based generator architecture for generative adversarial networks," in *Proceedings of the IEEE Conference on Computer Vision and Pattern Recognition (CVPR)*, 2019, pp. 4396–4405.

[33] S. Baliah, Q. Lin, S. Liao, X. Liang, and M. H. Khan, "Realistic and efficient face swapping: A unified approach with diffusion models," in *Proceedings of the Winter Conference on Applications of Computer Vision (WACV)*, February 2025, pp. 1062–1071.

[34] D. Hendrycks and K. Gimpel, "A baseline for detecting misclassified and out-of-distribution examples in neural networks," *Proceedings of International Conference on Learning Representations*, 2017.

[35] T. DeVries and G. W. Taylor, "Learning confidence for out-of-distribution detection in neural networks," *arXiv preprint arXiv:1802.04865*, 2018.

[36] D. P. Kingma and J. Ba, "Adam: A method for stochastic optimization," in *Proceedings of the International Conference on Learning Representations (ICLR)*, May 2015, pp. 1–15.

[37] B. Zi, M. Chang, J. Chen, X. Ma, and Y.-G. Jiang, "Wilddeepfake: A challenging real-world dataset for deepfake detection," in *Proceedings of the 28th ACM International Conference on Multimedia*, 2020, pp. 2382–2390.

[38] Y. Li, X. Yang, P. Sun, H. Qi, and S. Lyu, "Celeb-df: A large-scale challenging dataset for deepfake forensics," in *2020 IEEE/CVF Conference on Computer Vision and Pattern Recognition (CVPR)*, 2020, pp. 3204–3213.

[39] B. Dolhansky, J. Bitton, B. Pflaum, J. Lu, R. Howes, M. Wang, and C. Canton-Ferrer, "The deepfake detection challenge dataset," *arXiv preprint arXiv:2006.07397*, 2020.

[40] L. Jiang, R. Li, W. Wu, C. Qian, and C. C. Loy, "Deeperforensics-1.0: A large-scale dataset for real-world face forgery detection," in *Proceedings of the IEEE Conference on Computer Vision and Pattern Recognition (CVPR)*, June 2020, pp. 2886–2895.

[41] L. Van der Maaten and G. Hinton, "Visualizing data using t-sne." *Journal of machine learning research*, vol. 9, no. 11, 2008.

[42] K. Narayan, V. VS, and V. M. Patel, "Segface: Face segmentation of long-tail classes," *arXiv preprint arXiv:2412.08647*, 2024.

[43] R. R. Selvaraju, M. Cogswell, A. Das, R. Vedantam, D. Parikh, and D. Batra, "Grad-cam: Visual explanations from deep networks via gradient-based localization," in *Proceedings of the IEEE International Conference on Computer Vision (ICCV)*, October 2017, pp. 618–626.